AIAA JOURNAL
Vol. 45, No. 5, May 2007

Flexible Flapping Airfoil Propulsion at Low Reynolds Numbers

S. Heathcote* and I. Gursul†
University of Bath, Bath, BA2 7AY England, United Kingdom

DOI: 10.2514/1.25431

Water tunnel experiments on chordwise-flexible airfoils heaving with constant amplitude have been carried out for Reynolds numbers of 9,000 to 27,000. A degree of flexibility was found to increase both thrust coefficient and propulsive efficiency. Measurements of the flow field revealed stronger trailing-edge vortices corresponding to higher thrust coefficients, and weaker leading-edge vortices corresponding to higher efficiencies. By analogy with a rigid airfoil in coupled heave and pitch, thrust coefficient and propulsive efficiency were found to be functions of the Strouhal number and pitch phase angle. Propulsive efficiency peaks at a pitch phase angle of 95–100 deg (consistent with experimental and computational simulations of rigid airfoils in coupled heave and pitch), and a Strouhal number of 0.29, which lies in the middle of the range observed in nature. Thrust peaks at pitch phase angles in the region of 110–120 deg, but at higher Strouhal numbers. The results suggest the effect of chordwise flexibility is beneficial for purely heaving airfoils at low Reynolds numbers.

Nomenclature

a	=	amplitude
b	=	plate thickness
C_P	=	time-averaged power-input coefficient
C_T	=	time-averaged thrust coefficient
c	=	chord length
E	=	modulus of elasticity
h	=	dimensionless leading-edge amplitude (a_{LE}/c)
K	=	thin plate bending stiffness ($\mathrm{Eb}^3/12$)
Re	=	Reynolds number ($U_0 c/\nu$)
s	=	displacement
Sr	=	Strouhal number ($2fa_{\mathrm{LE}}/U_0$)
t	=	time
T	=	thrust; period
U_0	=	freestream velocity
V	=	velocity magnitude
v	=	airfoil leading-edge velocity
x	=	streamwise position
y	=	cross-stream position
α	=	effective angle of attack [$\tan^{-1}(v/U_0) - \theta$]
η	=	efficiency
λ	=	bending stiffness coefficient
μ	=	viscosity
ν	=	kinematic viscosity (μ/ρ)
θ	=	pitch angle
ρ	=	density
ω	=	heave angular frequency
Ω	=	vorticity

Subscripts

LE	=	leading edge
TE	=	trailing edge

Presented as Paper 2005-1405 at the 43rd AIAA Aerospace Sciences Meeting and Exhibit, Reno, NV, 10–13 January 2005; received 26 May 2006; revision received 13 September 2006; accepted for publication 13 September 2006.

*Graduate Student, Department of Mechanical Engineering. Student Member AIAA.

†Professor, Department of Mechanical Engineering. Associate Fellow AIAA.

I. Introduction

THERE is a wish to build miniature aircraft known as micro air vehicles (MAVs) for which numerous applications have been cited. One example is to relay video pictures from the source of a leak on an offshore oil rig. A second example is to relay sound and picture in "over the hill" reconnaissance situations. Some MAVs have already been constructed [1–3]. It is thought that it may be possible to approach the agility and endurance of birds and insects by adopting a flapping wing mechanism [4], and for this reason there is a need to understand the aerodynamics of oscillating airfoils. The key aerodynamic parameter is the Reynolds number [5]. Because the length scale of birds, insects, and MAVs is of the order of the centimeter, the Reynolds number is very low, typically $Re = 10^3$–10^5, and an understanding of the nature and relative importance of inviscid and viscous phenomena in this regime is sought.

The first scientific explanation of bird flight was given by Knoller [6] in 1909. He described how the flapping motion of an airfoil would give rise to oscillatory lift and thrust forces. The work was repeated independently by Betz [7], and published shortly afterwards in 1912. In his findings, Betz described the potentially positive effect of air turbulence. Vertical oscillations of the air flowing over a gliding bird's wing were shown to generate a force in the direction of flight, thereby reducing the drag. Wind tunnel experiments by Katzmayr [8] verified what is now known as the Knoller–Betz effect. In the manner of Betz, the wing in Katzmayr's experiment was stationary, and the oscillations were of the air. In 1936, Garrick [9] published a set of equations for the thrust and efficiency of a flat plate oscillating in inviscid flow. Pure heave, pure pitch, and coupled heave and pitch motions were modeled, although the equations are valid only in the limit of small amplitude oscillations. Other key inviscid studies were by Wu [10], Lighthill [11], and Chopra [12], the last of whom extended Garrick's theory to oscillations of arbitrary amplitude. An inviscid panel method was developed and applied by Jones et al. [13] to a heaving NACA0012 airfoil. Jones et al. [13] found a remarkable similarity between the flow patterns predicted by the panel method and those observed in experiments, illustrating how the formation of a reverse von Kármán street for an oscillating airfoil is essentially an inviscid phenomenon. These inviscid methods are valid in the case of high Reynolds number and small local (or *effective*) angles of attack. At the low Reynolds numbers of birds, insects, fish, and MAVs, flow separation tends to occur at the leading edge [14], especially at high angles of attack. Inviscid methods are not capable of predicting such flow separation effects and, for this reason, Navier–Stokes codes have been developed. These methods are able to predict leading-edge flow separation, vortex formation and shedding, and the consequent merger of the leading-edge vortices into the trailing-edge vortex

system. The propulsive efficiency of oscillating airfoils has been shown to depend greatly on these effects, and in general to be rapidly degraded by the onset of leading-edge flow separation [15–18]. These Navier–Stokes simulations show that efficiency is degraded by the formation of leading-edge vortices. For example, Tuncer and Platzer [16] observed the transition from weakly separated leading-edge flow to the shedding of large scale leading-edge vortices to correspond to a sharp decline in efficiency. The diminished efficiency was attributed to both a rise in power input (because of the suction effect of the leading-edge vortex) and a fall in thrust (because of the disruption to the reverse vortex street caused by the arrival of the leading-edge vortex). Peak efficiencies occur at angles of attack sufficiently small that such a phenomenon occurs only very weakly.

The airfoils in the majority of experimental studies have been rigid. Of these studies, the majority have been carried out at low Reynolds numbers, although a number have modeled hovering flight [19–21] ($U_0 = 0$). A number of experimental techniques [22–26] have been used, including force balance measurements of thrust and efficiency, particle image velocimetry and molecular tagging velocimetry measurements of the velocity field, and dye and smoke visualization. A variety of different oscillating motions have been investigated, including harmonic heave [13], harmonic pitch [27], coupled heave and pitch [22], and also alternative displacement waveforms to the cosine wave (e.g., triangle waveform) [28]. Introducing a pitch motion to the heave of rigid airfoils has been found to yield potentially higher efficiencies. The mechanism has been found to be the diminishing of the leading-edge vortex [16,29] through a lower effective angle of attack. The coupled heave and pitch motion is of interest in studies of nature, particularly in the thunniform swimming [30] of, for example, tuna, swordfish, and dolphins.

If we are to be guided by nature in the design of miniature aircraft, then it becomes necessary to study birds and insects in more detail. One question is of the stiffness of their wings. Studies of insect wings by Wootton [31] and Steppan [32] have revealed intricate variations in their stiffness. However, although areas of the wing have been identified as being specifically flexible [31], how this benefits the insect aerodynamically is still not clear [33]. Flexibility is an interesting subject in the design of MAVs, because in addition to any aerodynamic benefits it is noted that flexible wings are inherently light. The subject of flexibility in the arena of oscillating airfoils is relatively unexplored, however, despite the knowledge that it is of importance in bird and insect flight, and essential in fish swimming [34]. Numerical models have indicated higher efficiencies for flexible airfoils [35–37], though the computational complexity of the situation requires assumptions either of inviscid flow [35] or of a predefined flexing motion [37,38]. Experimentally, there are findings of higher thrust at zero freestream Reynolds number (the special case of hovering flight) [39,40], and of higher efficiency at nonzero Reynolds numbers [41]. A systematic study of the effect of airfoil deformation on the flow field and force coefficients is absent from the literature, however.

The aim of the present study is to examine the flow-structure interaction, thrust, and efficiency of a flexible 2-D airfoil oscillating in heave at low Reynolds numbers. A chordwise-flexible airfoil (Fig. 1) is oscillated in heave with constant amplitude. It is noted that the shape of the airfoil follows the observations of Wootton [31] that bird's wings have relatively stiff leading edges, and resembles the airfoil of the MAV of Jones et al. [42], and in some ways the tadpole in the CFD study of Liu et al. [43]. Unlike experimental studies of rigid airfoils in coupled heave and pitch, the pitching motion arises naturally through chordwise flexibility.

Four appropriate parameters are Re, h, Sr, and λ. The Reynolds number is based on the chord length of the airfoil. The dimensionless heave amplitude $h = a_{\mathrm{LE}}/c$ is based on the amplitude of the leading edge. The Strouhal number is based on the peak-peak amplitude of the leading-edge. This definition is found throughout the literature [28,29,41]. Physically, for an airfoil in pure heave, the Strouhal number is related to the effective angle of attack. The parameter has been shown to be significant in the study of the wake pattern from a heaving airfoil [24], and in particular whether the wake pattern is

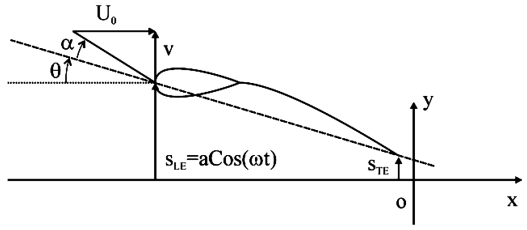

Fig. 1 Schematic of the flexible airfoil heaving periodically in the vertical direction.

characteristic of net thrust, drag, and lift [13]. It has also been found to have significance in nature, where the Strouhal numbers of insects, birds, bats, and fish are observed to lie within a narrow range [44] of $0.2 < Sr < 0.4$. The bending stiffness parameter is defined following the approach of Murray [45] as

$$\lambda = \frac{K}{\frac{1}{2}\rho U_0^2 c^3}$$

II. Apparatus

Experiments were carried out in water with two airfoils: a 400 mm span, 100 mm chord, NACA0012 airfoil, inflexible in both the spanwise and chordwise directions, and a 300 mm span, 90 mm chord, teardrop/flat plate design (Fig. 1), flexible in the chordwise direction only. The plate was a sheet of steel of uniform thickness of modulus of elasticity 2.05×10^{11} N/m^2 and length 60 mm. The teardrop element was of chord 30 mm, thickness 10 mm, and solid aluminum. The purpose of the experiments on the NACA0012 airfoil was to validate the force measurements. The second teardrop/plate airfoil allowed for a study of chordwise flexibility by varying the thickness of the carbon–manganese steel plate. Experiments were carried out on 7 plates, identical apart from their thickness. The bending stiffness of the plates relative to the most flexible airfoil, $b/c = 0.56 \times 10^{-3}$, is shown in Table 1.

Experiments were conducted in a free-surface closed-loop water tunnel (Eidetics model 1520) with a 381 mm wide × 508 mm deep test section and flow speed range of 0–0.45 m/s (see Fig. 2). Experiments were performed for tunnel speeds of 0.1, 0.2, and 0.3 m/s corresponding to Reynolds numbers based on the chord length of the 90 mm airfoil of 9,000, 18,000, and 27,000, respectively. The free stream velocity was measured with a TSI laser Doppler velocimetry system in back scatter mode. The airfoil was mounted vertically with one end attached to a horizontal shaker (Motovario 0.37 kW three-phase motor, 5:1 worm gear and IMO Jaguar controller). Perspex splitter plates were positioned 2 mm above and below the airfoil. The displacement of the leading-edge was given by $s_{\mathrm{LE}} = a_{\mathrm{LE}} \cos(\omega t)$. The displacement of the airfoil was measured with a position sensor attached to the output shaft of the worm gear. Tests were carried out for frequencies in the range of 0.29–2.54 Hz. Experiments on the effect of chordwise flexibility were carried out at constant amplitude, $a = 17.5$ mm. Force validation experiments on the NACA0012 airfoil were carried out for amplitudes in the range 12.5 mm $< a <$ 20 mm. A binocular strain gauge force balance [46], machined from aluminum, was used to make direct force measurements in directions parallel and perpendicular to the freestream velocity.

Table 1 Bending stiffness of plates relative to the most flexible airfoil, $b/c = 0.56 \times 10^{-3}$

Plate thickness, b/c	Relative stiffness, λ/λ_0
0.56×10^{-3}	1
0.84×10^{-3}	3.4
1.12×10^{-3}	8
1.41×10^{-3}	15.6
1.69×10^{-3}	27
2.25×10^{-3}	64
4.23×10^{-3}	422

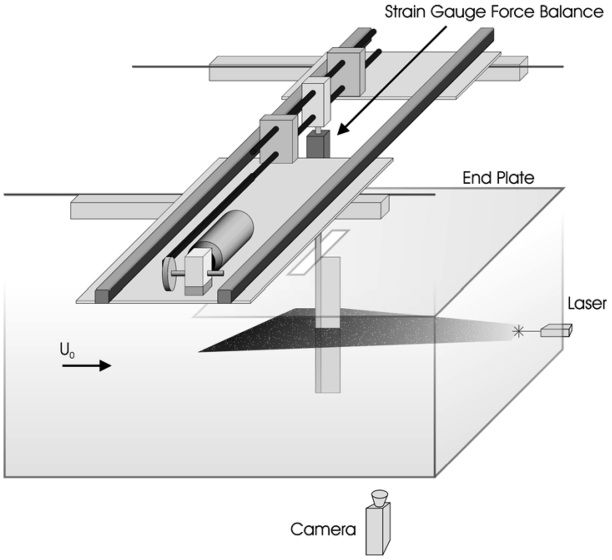

Fig. 2 Water tunnel experimental setup for force measurement, particle image velocimetry, and measurement of the displacements of the leading and trailing edges.

III. Experimental Methods

A. Force Measurement

The forces applied to the wing in the "x" and "y" directions, "F_x" and "F_y", were measured with a binocular strain gauge force balance. The force F_x is equal to the drag (or thrust) on the wing. The force F_y is equal to the lift "L" on the wing, plus a contribution arising from the inertia of the wing. This contribution is proportional to the mass "m" of the wing and the wing acceleration in the y-direction ($\mathrm{d}v/\mathrm{d}t$), in which "v" is the instantaneous plunging velocity. Hence, total force measured is $F_y = L + m\,\mathrm{d}v/\mathrm{d}t$ and the power input can be calculated as $Lv = (F_y - m\,\mathrm{d}v/\mathrm{d}t)v$. On integrating with time over a complete heave cycle, the term $v\,\mathrm{d}v/\mathrm{d}t$ vanishes because the phases of v and $\mathrm{d}v/\mathrm{d}t$ differ by 90 deg. Hence the inertia of the airfoil does not contribute to the time-averaged power input. This approach of using F_y for the input power calculations was validated as will be discussed later in the paper.

Driving force and thrust force data were collected for 60 oscillations (sample rate 1 kHz) for each test condition. The thrust coefficient is given by

$$C_T = \frac{T}{\frac{1}{2}\rho U_0^2 c}$$

in which "T" is the time-averaged thrust per unit span. The time-averaged power input is given by

$$C_P = \frac{\overline{F_y v}}{\frac{1}{2}\rho U_0^3 c}$$

in which "$F_y v$" is the instantaneous power input, and the overbar denotes an average over time. The propulsive efficiency is given by

$$\eta = \frac{TU_0}{\overline{F_y v}} = \frac{C_T}{C_P}$$

B. Force Measurement Uncertainty

Because the fluid dynamic forces acting on the wing may vary along the span, it is important that the force balance is sensitive only to force, and insensitive to the distance from the gauge at which the force acts. Insensitivity to bending moment is a key feature of a binocular strain gauge force balance. It was found during the calibration tests that the uncertainty in F_x and F_y induced by a typical range of bending moments was less than 0.5%. Coupling effects (fictitious indicated forces in the x direction due to loading in the y direction, and vice versa) were found to give rise to a 2% uncertainty. The uncertainty due to torque about the z axis was found to be 1%. The uncertainty from temperature variations was found to be negligible. The response of the gauge was found to be linear (1% uncertainty) over the experimental range. The combined uncertainty in the strain gauge readings is approximately 3%. Because the efficiency readings depend on readings of both F_x and F_y, the uncertainty in the efficiency data is approximately 6%.

C. Force Measurement Validation

To validate the force measurement system, a set of thrust and power-input measurements were carried out for a 100 mm chord, 400 mm span, NACA0012 airfoil, oscillating with constant amplitude ($h = 0.175$) between splitter plates. Tests were carried out for Reynolds numbers of 10,000, 20,000, and 30,000, and for a frequency range of $0 < Sr < 0.72$. The thrust coefficient, power-input coefficient, and propulsive efficiency data are plotted in Figs. 3a, 3b, and 4, respectively. Also shown for comparison are the predictions of Garrick theory [9], a panel method [47], and a viscous Navier–Stokes code [48] (run for $Re = 20,000$, M $= 0.05$, laminar flow). To match the parametric range of the present experimental data, additional calculations were performed by Young.[‡]

It is seen from Fig. 3a that the Navier–Stokes predictions for thrust coefficient are in very close agreement with the experimental values over the complete frequency range. Furthermore, close agreement is found between the measured drag coefficient ($C_D = 0.028$) and the values found in previous experiments by Sheldahl and Klimas [49] ($C_D = 0.0245$) and Koochesfahani [27] ($C_D = 0.027$). A number of additional observations may be made in Fig. 3a. First, the experimental data show the effect of Reynolds number to be very small for the range $10,000 < Re < 30,000$. Second, the panel method predicts marginally higher thrust coefficients than Garrick theory, consistent with the findings of Jones et al. [50]. Both inviscid methods overestimate the experimentally measured thrust coefficient.

It is seen in Fig. 3b that close agreement is observed between the experimental and Navier–Stokes predictions for power-input coefficient. Here again, the effect of Reynolds number is observed to be small for the experimental data. Garrick theory and the panel method are seen to underestimate the power-input coefficient, particularly severely in the case of Garrick theory. Young [48] showed the key limitation of the panel method to be the absence of a model of leading-edge vorticity shedding; leading-edge vortices in the Navier–Stokes model were shown to augment the surface pressures, leading to a greater power-input requirement. This limitation is shared by Garrick theory, which is further afflicted, as described by Jones et al. [50], by an overly simplistic model of the shedding of trailing-edge vorticity.

Propulsive efficiency (the ratio of thrust coefficient to power-input coefficient) is shown in Fig. 4. Although the panel method correctly predicts a decrease in efficiency with increasing frequency (Garrick theory predicts the efficiency to tend to a value of 0.5), both inviscid methods are seen to significantly overestimate efficiency. It is seen from Fig. 3 that the inaccuracy of the inviscid methods results primarily from the power-input coefficient predictions. Reasonable agreement is observed between the experiments and Navier–Stokes simulations. In particular, close agreement is found in the trend toward drag (negative efficiency) at low frequencies, the peak efficiency ($\eta \approx 30\%$), and the optimum frequency ($Sr \approx 0.1$).

D. Displacement

The oscillating wing was filmed with a 50 frames-per-second high-shutter-speed video camera (see Fig. 2). Specialist motion-tracking software (RealViz MatchMover Pro 3.1) returned the coordinates of the leading edge and trailing edge in each frame. After the initial transients, the positions of the edges (and the "pitch" angle of the airfoil) were recorded over four oscillations. The phase and amplitude of the leading-edge, the trailing-edge, and the pitch angle, were found with a cosine fit.

[‡]Young, J., private communication., 2006.

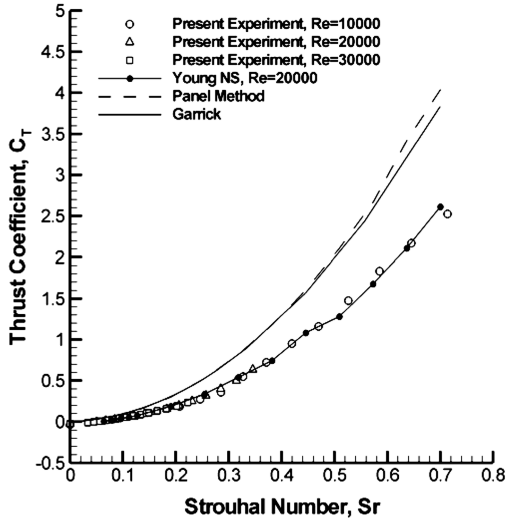

a)

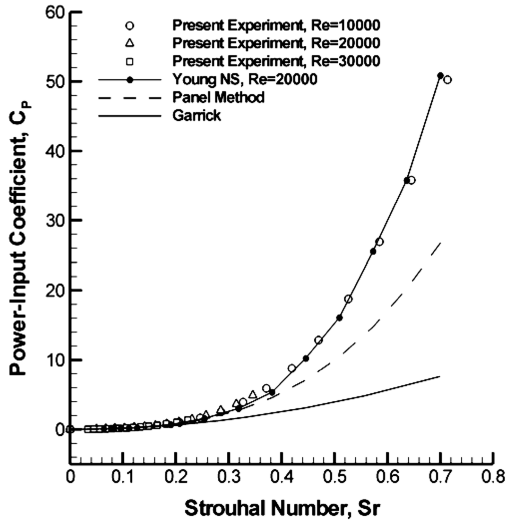

b)

Fig. 3 Comparison of present experimental data with linear theory, panel method, and Navier–Stokes solver; NACA0012 airfoil in pure heave (except Garrick, thin airfoil), $h = 0.175$: a) thrust coefficient; b) power-input coefficient.

E. Particle Image Velocimetry

Particle image velocimetry measurements were taken with a TSI particle image velocimetry (PIV) system. Nylon particles of 4 μm diameter were used for seeding. The PIV system comprised an 8-bit gray scale digital camera, dual mini Nd:Yag 120 mJ pulsed laser, remote focusing apparatus, synchronization unit, SCSI image acquisition card, dual Xeon processor computer, and Insight 6 image processing software. Images were captured at a rate of 3.75 pairs per second, and with a resolution of 2048×2048 pixels. The separation of laser pulses was 500 μs. A fast-Fourier-transform algorithm was used to analyze the image pairs. A window size of 32×32 pixels with 50% overlapping was chosen, to give 127×127 velocity vectors with spatial resolution 0.016c. Time-averaged flow fields were obtained by taking an average of 256 velocity fields. Phase-averaged flow fields were obtained by taking an average of 200 velocity fields. The uncertainty in the velocity measurements was estimated to be around 2%.

IV. Results

The following sections present the results for the chordwise-flexible airfoil, in which the effect of airfoil stiffness is investigated. Thrust coefficient and efficiency are studied first as functions of plate thickness, Strouhal number and Reynolds number and then, following analysis of the deformation characteristics of the airfoil, as functions of *pitch phase angle*, Strouhal number and Reynolds number. Optimum pitch phase angles for thrust and efficiency are found, and compared with those in the literature. Flow fields are shown throughout, to illustrate how trends in thrust and efficiency relate to changes in the flow pattern.

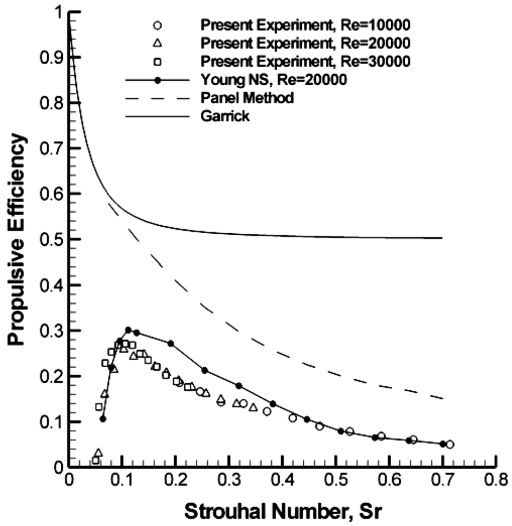

Fig. 4 Comparison of propulsive efficiency data with linear theory, panel method, and Navier–Stokes solver; NACA0012 airfoil in pure heave (except Garrick, thin airfoil).

It is found that the thrust coefficient of a heaving airfoil increases rapidly with Strouhal number. According to Garrick [9], the thrust coefficient of a flat plate in pure heave (valid in the limit of small amplitude oscillations) is given by

$$C_T = \pi^3 Sr^2 (F^2 + G^2)$$

in which F and G are the real and imaginary parts of the Theodorsen lift deficiency function. For this reason the quantity C_T/Sr^2 is sometimes chosen in preference to C_T alone [28]. An alternative method is to define a thrust coefficient $T/(\frac{1}{2}\rho v_p^2 \mathrm{S}) \equiv C_T/(\pi Sr)^2$, in which v_p is the peak heave velocity of the airfoil [15]. This approach has been taken in studies of hovering flight [19,39] ($U_0 = 0$), in which the conventional formulation of thrust coefficient is undefined. From here on, the quantity C_T/Sr^2 will be plotted.

A. Effect of Airfoil Stiffness on Thrust

The remainder of this paper focuses on the effect of chordwise flexibility. All experimental results from this point forward are for the chordwise-flexible airfoil shown in Fig. 1. The variation of thrust coefficient divided by the square of the Strouhal number C_T/Sr^2 with plate thickness is plotted in Fig. 5. Plots are shown for a) $Re = 9,000$, b) $Re = 18,000$, and c) $Re = 27,000$ (the zero Reynolds number case has been studied before [39]). Measurements are taken for seven plates of different thickness. For each Reynolds number, and for each Strouhal number, a peak in the thrust coefficient is observed. The peak moves to higher values of plate thickness with increasing Strouhal number. For high Strouhal numbers, the optimum thickness may be exceeded without a severe degradation in performance, although a sharp decline in thrust coefficient occurs if the airfoil is too thin. The results indicate that flexibility improves the thrust performance of the airfoil at low Reynolds numbers. Note that, although the Strouhal number range decreases with increasing Reynolds number, the oscillation frequencies, in Hertz, are the same for parts a), b), and c).

The features of the wake for rigid and flexible airfoils may be illustrated with example velocity and vorticity fields for $Re = 9,000$, $Re = 18,000$, and $Re = 27,000$. Three velocity fields are shown in Fig. 6 for $Re = 9,000$. The outline of the airfoil is drawn, and velocity vectors in the plane of the midspan of the airfoil are shown. The position of the leading edge in each part, $s = +a$, corresponds to

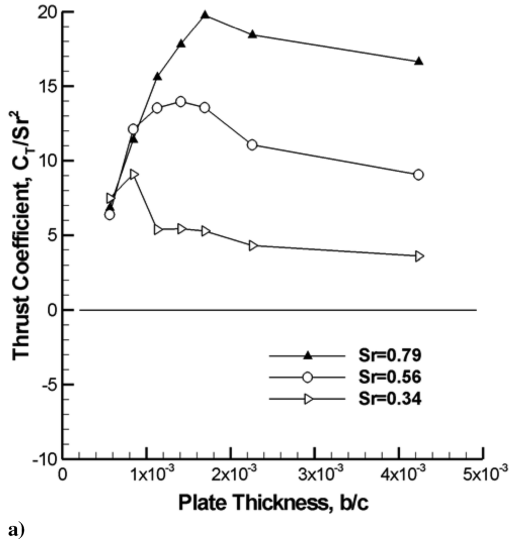

a)

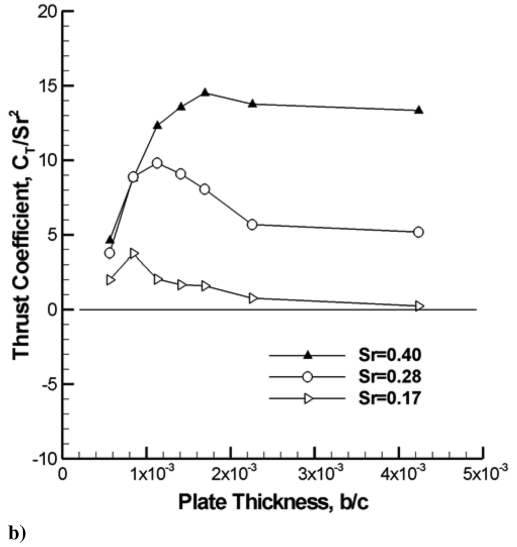

b)

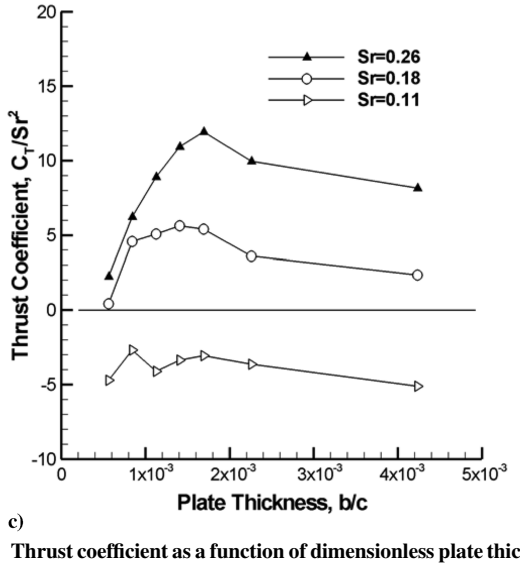

c)

Fig. 5 Thrust coefficient as a function of dimensionless plate thickness: a) $Re = 9,000$; b) $Re = 18,000$; c) $Re = 27,000$.

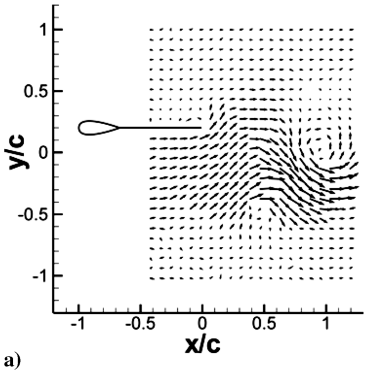

a)

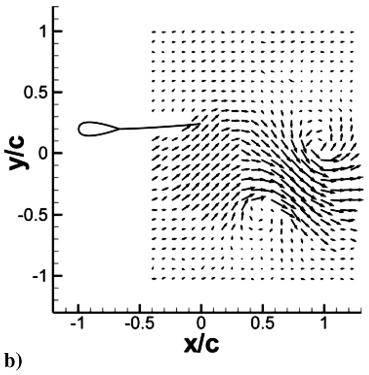

b)

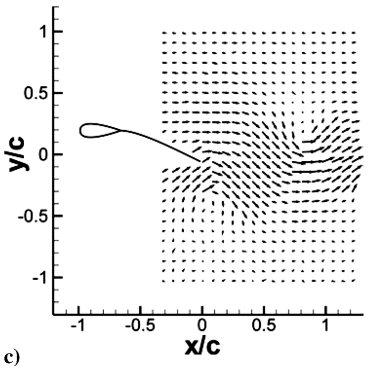

c)

Fig. 6 Instantaneous velocity fields at $t/T = 0$ for $Re = 9,000$, $Sr = 0.56$: a) $b/c = 4.23 \times 10^{-3}$; b) $b/c = 1.41 \times 10^{-3}$; c) $b/c = 0.56 \times 10^{-3}$. The time-averaged thrust coefficient is greatest in part b).

a time $t/T = 0$. The three parts in Fig. 6 correspond to three different plate thicknesses in the $Sr = 0.56$ curve of Fig. 5a. Differences exist between parts a), b), and c) in the shape of the airfoil and in the velocity field. In the case of the stiffest plate (Fig. 6a), the *pitch angle* of the airfoil, defined by the angle between the freestream and a chordline drawn from the leading edge to the trailing edge, is less than 1 deg; the airfoil is essentially rigid. The *pitch amplitudes* of the intermediate [part b)] and highly flexible airfoil [part c)] are 6 and 17 deg, respectively. As expected, the pitch amplitude increases with plate flexibility. A more subtle difference exists between the airfoils in parts b) and c): whereas for the case of intermediate stiffness the airfoil pitches down at $t/T = 0$, the reverse is true of the most flexible airfoil. In this way it is seen that the stiffness of the plate affects both the pitch amplitude and the *pitch phase angle*. It is shown later that a relationship exists between pitch phase and pitch amplitude. The thrust coefficient is greatest for the airfoil of intermediate flexibility (Figs. 5a and 6b); the vortices from this airfoil are stronger, and further apart in the lateral (y) direction. It is noted that vortex pairs (vortex dipoles) are observed for the stiffest and intermediate airfoils.

Time-averaged velocity magnitude contours for the three airfoils are shown in Fig. 7. The peak jet velocity and jet width are seen to be highest for the airfoil of intermediate plate thickness, consistent with the force data. The jets from the intermediate and greatest stiffness airfoils lie at an angle to the freestream direction. The vortices in these two cases are shed in pairs. Such deflected jets have been found to occur when the Strouhal number exceeds a critical value [13].

Vorticity fields for three airfoils of different plate thickness are shown in Fig. 8 for $Re = 18,000$. The leading edge of the airfoil is moving upwards through the origin ($t/T = \frac{3}{4}$). Each *phase-averaged* vorticity field was calculated from a series of 200 velocity fields, each

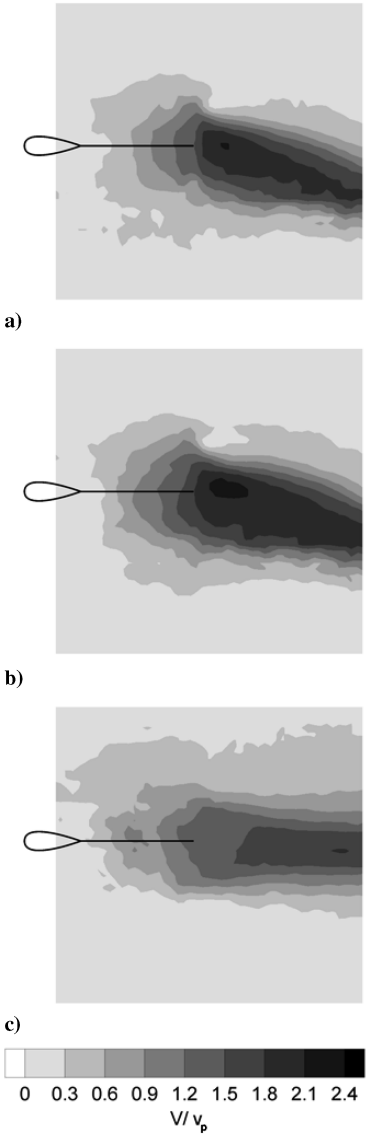

Fig. 7 Time-averaged velocity fields corresponding to Fig. 6.

captured at the same point in the oscillation. Clockwise vorticity is shown white, counterclockwise vorticity black. It is noted that, whereas vortex pairs were observed in the $Re = 9,000$ case, a reverse vortex street, parallel to the freestream, is observed in the present case. This is attributed to the lower Strouhal number. The highest thrust coefficient occurs for the airfoil of intermediate stiffness [part b)]. It is seen that the vortices from the intermediate airfoil are stronger, and spaced further apart in the lateral direction than those from the stiffest airfoil. Although a large distance in the lateral direction separates the vortices from the least stiff airfoil, their strength is considerably lower than for either of the other two airfoils.

Velocity magnitude and vorticity contour fields for the three airfoils are shown in Fig. 9 for $Re = 27,000$. Again, the leading edge is moving upwards through the origin. Gray levels in Fig. 9 indicate velocity magnitude; white lines indicate contours of vorticity (solid for clockwise flow, dotted for counterclockwise flow). The highest thrust coefficient occurs for the airfoil of intermediate stiffness [part b)]. In this case it is seen that a large lateral distance separates the regions of opposite vorticity. It is noted that the vortices from the most flexible airfoil are shed almost in a line. The measured thrust coefficient $C_T = 0.04$ is correspondingly small.

B. Effect of Oscillation Frequency on Thrust

Plots of thrust coefficient against Strouhal number are shown in Fig. 10 for five plate thicknesses. Plots are shown for a) $Re = 9,000$, b) $Re = 18,000$, and c) $Re = 27,000$. With the appropriate choice of airfoil, benefits to flexibility are observed over the complete Reynolds and Strouhal number range. Peaks in thrust coefficient are observed in some cases, although not as markedly as in the plots of thrust coefficient against plate thickness. The peaks are seen to move to higher Strouhal numbers with increasing plate stiffness. For all Reynolds numbers, a transition from drag to thrust occurs for the stiffest, essentially rigid, airfoil, at a Strouhal number $Sr \approx 0.17$, and earlier for the flexible airfoils.

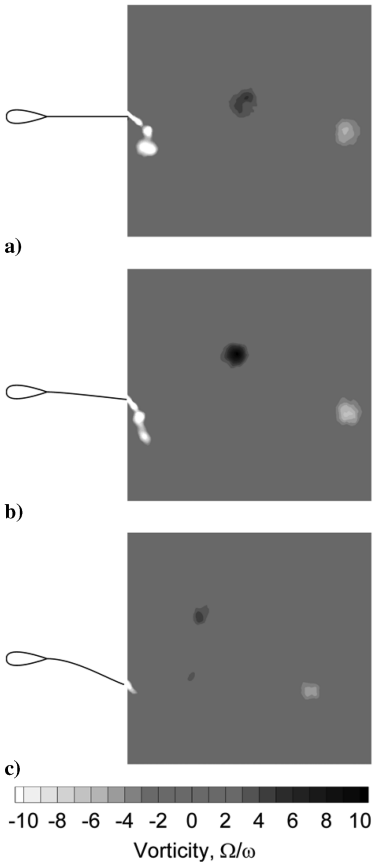

Fig. 8 Phase-averaged vorticity fields for three airfoils; $Re = 18,000$, $Sr = 0.26$, 200 capture average: a) $b/c = 4.23 \times 10^{-3}$; b) $b/c = 1.13 \times 10^{-3}$; c) $b/c = 0.56 \times 10^{-3}$. The thrust coefficient is greatest in part b).

Instantaneous vorticity contour plots corresponding to the $b/c = 0.85 \times 10^{-3}$ curve in Fig. 10a are shown in Fig. 11. Note that the vorticity is normalized with frequency as Ω/ω to explore the effect of Strouhal number. The stiffness of the airfoil is the same for each plot, and the frequency is incremented from part a) to part c). The leading edge is moving upwards through the origin in each part. As expected, the pitch angle of the airfoil at this instant increases with increasing Strouhal number. The pitch angle of the airfoil undergoing the lowest frequency oscillation is around 1 deg. The vortices in the intermediate frequency case (maximum thrust coefficient) are seen to be stronger, and separated by a greater lateral distance, than the vortices of the low frequency case. In the high frequency case (Fig. 11c), vortices are shed in pairs. This is commensurate with the higher Strouhal number effects [13]. It is seen that the jet is deflected slightly away from the freestream direction.

Time-averaged velocity magnitude plots for the three Strouhal numbers in Fig. 11 are shown in Figs. 12b, 12d, and 12f . Additional frequencies are plotted in Figs. 12a, 12c, and 12e. The shading indicates the velocity magnitude normalized by the peak leading-edge heave velocity. The difference between the maximum jet velocity and the velocity of the surrounding flow is relatively small at low Strouhal numbers, but becomes larger with increasing Sr. The strength of the jet is seen to grow with frequency, reach a maximum around $Sr = 0.41$–0.48, and then decay. The frequency for which the strongest jet is observed corresponds to the peak in thrust

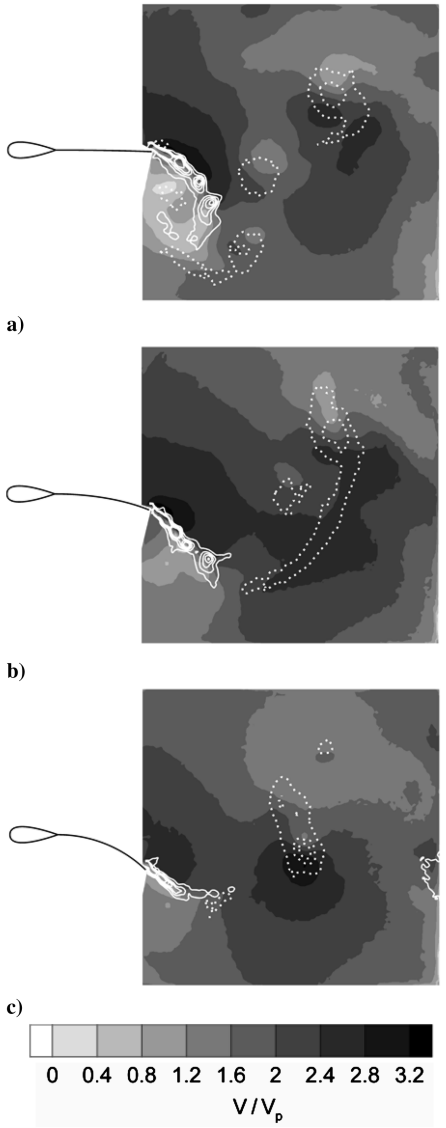

Fig. 9 Phase-averaged velocity magnitude (gray scale) and vorticity (clockwise: solid white lines; counterclockwise: dotted white lines; first level: $\Omega/\omega = 0.85$; increment: $\Omega/\omega = 1.9$) for three airfoils; $Re = 27,000$, $Sr = 0.17$: a) $b/c = 4.23 \times 10^{-3}$; b) $b/c = 1.13 \times 10^{-3}$; c) $b/c = 0.56 \times 10^{-3}$. The thrust coefficient is greatest in part b).

coefficient (Fig. 12d). In Figs. 12e and 12f, a deflected jet (seen in the instantaneous vorticity field of Fig. 11c) is characteristic of the high Strouhal number effects mentioned earlier.

C. Efficiency

Propulsive efficiency is plotted as a function of Strouhal number in Fig. 13 for a) $Re = 9,000$, b) $Re = 18,000$, and c) $Re = 27,000$. Cases of negative efficiency (drag) are not shown. Curves for five plate thicknesses are shown to illustrate the effect of airfoil stiffness. It is seen that the efficiency of the flexible airfoils is significantly higher than the efficiency of the stiffest, essentially rigid airfoil. Hence flexibility is seen to offer significant efficiency benefits, in addition to increases in thrust. For the $Re = 9,000$ case, the propulsive efficiency at low Strouhal numbers increases with increasing flexibility. It is possible that a still more flexible airfoil may yield even higher efficiencies. At the highest Strouhal number, it is one of the intermediate stiffnesses that yields the greatest efficiency. This trend is observed for all Reynolds numbers. A further trend is for the efficiency to move from positive to negative for the rigid airfoil at a Strouhal number of approximately 0.17 for each Reynolds number (consistent with the change from negative to positive thrust), and for the transition to positive efficiency to occur earlier for the flexible airfoils.

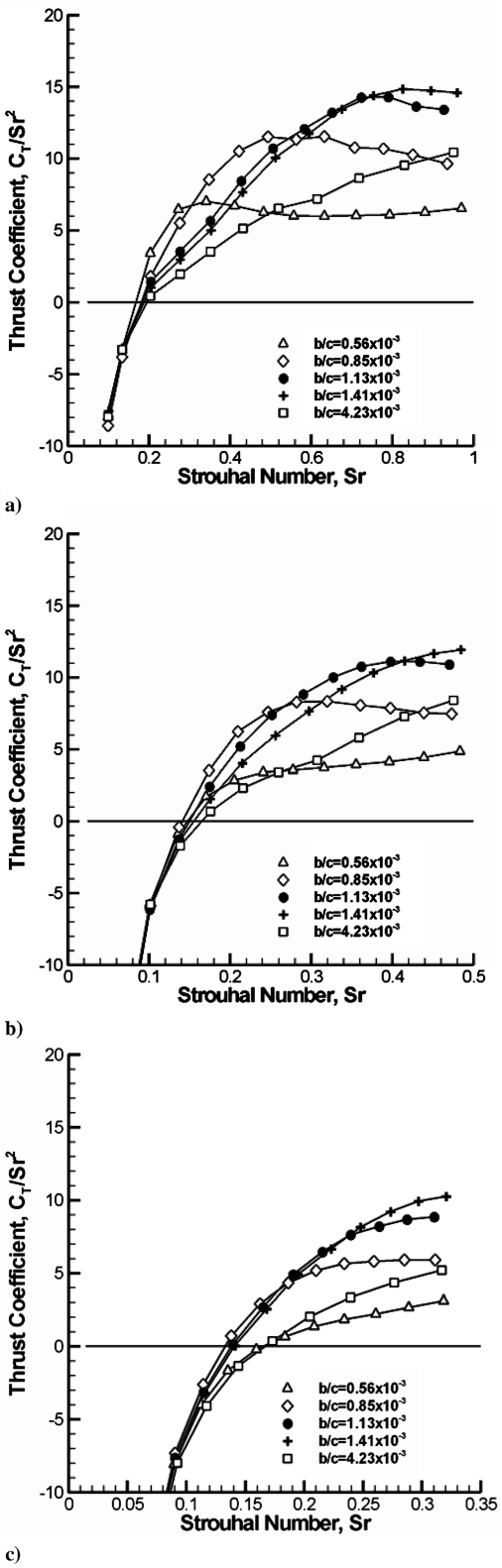

Fig. 10 Thrust coefficient as a function of Strouhal number: a) $Re = 9,000$; b) $Re = 18,000$; c) $Re = 27,000$.

As discussed earlier, the efficiency of oscillating airfoils is closely related to the flow near the leading edge. Flow separation has been shown to lead to significantly reduced propulsive efficiencies. It is therefore of interest to study the flow at the leading edge of the teardrop/plate airfoil, and to make a comparison between the rigid and flexible cases. The flow pattern over the airfoil for one complete oscillation is shown in Fig. 14 for times $t/T = 0, \frac{1}{4}, \frac{1}{2}, \frac{3}{4}$. The method is of dye flow visualization, and dye is released into the flow one chord

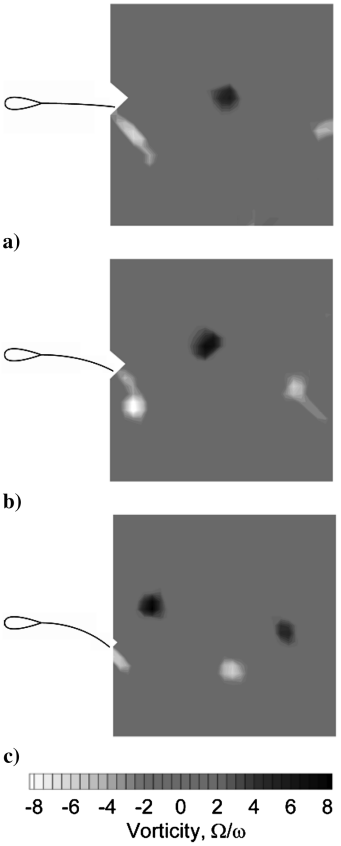

Fig. 11 Instantaneous vorticity fields for an airfoil oscillating at three frequencies; $Re = 9,000$, $b/c = 0.85 \times 10^{-3}$: a) $Sr = 0.27$; b) $Sr = 0.48$; c) $Sr = 0.97$. The thrust coefficient is greatest in part b).

length upstream of the leading edge. It is noted that the Reynolds number in Fig. 14 is chosen to yield the clear flow visualization images, and is lower than the Reynolds number of the thrust and efficiency measurements. However, the Strouhal number is typical of those in the force measurements. The airfoil is moving upwards through the origin in part a), reaches the highest displacement in part b), returns through the origin in part c), and reaches the lowest displacement in part d). The formation of both leading-edge and trailing-edge vortices is visible. Leading-edge vortices are observed to be shed in pairs, to convect downstream and be swept into the trailing-edge vortex pattern. Similar vortex shedding patterns have been simulated numerically by Lewin and Haj-Hariri [18], who found that although leading-edge vortices may be shed in pairs, the vortices of the pair tend to be unequal in strength. The manner in which the leading-edge vortices affect the efficiency has been explained in terms of the perturbation to the pressure distribution over the surface of the airfoil [48] and the disturbance they cause to the trailing-edge vortex system [18]. It has been shown that minimizing the strength of the leading-edge vortices is necessary to achieve high efficiency, and this is achieved through minimizing the effective angle of attack [15,17,29]. However, such small angles of attack tend to yield low thrust coefficients and a balance may therefore be sought between high efficiency and high thrust [17,29,51]. For a given Reynolds number and Strouhal number, it is interesting to compare the vortex shedding patterns for the airfoil stiffness that maximizes efficiency with the stiffness that maximizes thrust coefficient. Such a comparison is made in Fig. 15, in which the vorticity patterns of two airfoils are shown over one heave cycle, for $Re = 9,000$, $Sr = 0.34$. The two columns of images show vorticity magnitude fields at the same points in the cycle as Fig. 14. The first column of images is for the airfoil that experiences the greatest thrust coefficient. The second column of images is for a more flexible airfoil, which experiences the greatest efficiency. The formation and shedding of leading-edge vortices is visible in both cases, although those of the more flexible airfoil (column II) are observed to be

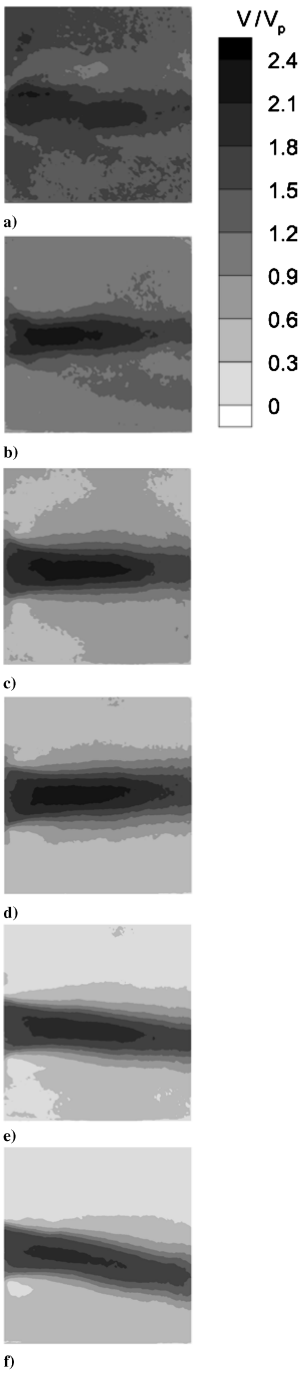

Fig. 12 Time-averaged velocity fields for a single-stiffness airfoil oscillating at six frequencies; $Re = 9,000$, $b/c = 0.85 \times 10^{-3}$: a) $Sr = 0.20$; b) $Sr = 0.27$; c) $Sr = 0.41$; d) $Sr = 0.48$; e) $Sr = 0.88$; f) $Sr = 0.97$.

weaker, both at the point of formation and further downstream where they are swept into the trailing-edge vortex pattern. This is consistent with the higher efficiency. In contrast, the trailing-edge vortex pattern is moderately stronger for the stiffer airfoil (column I). It is also noted that, as observed in the simulations of Lewin and Haj-Hariri [18], leading-edge vortices may be shed in pairs, with one dominant in strength.

D. Airfoil Shape Characteristics

A possibly more physically meaningful approach is to plot thrust coefficient against a shape characteristic of the airfoil, rather than against plate thickness. Pitch amplitude, pitch phase angle, and trailing-edge amplitude are possible parameters. A displacement-time plot for the single case $Re = 9,000$, $b/c = 0.56 \times 10^{-3}$, $Sr =$

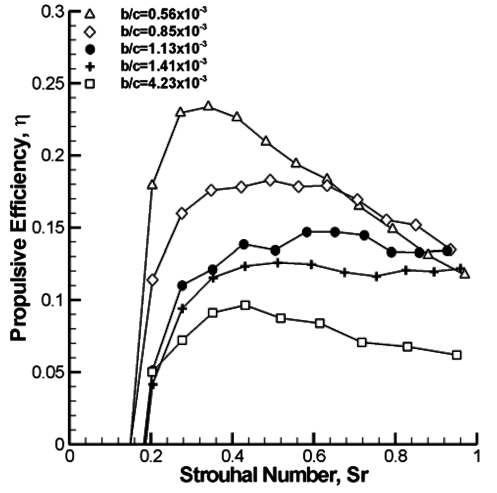

a)

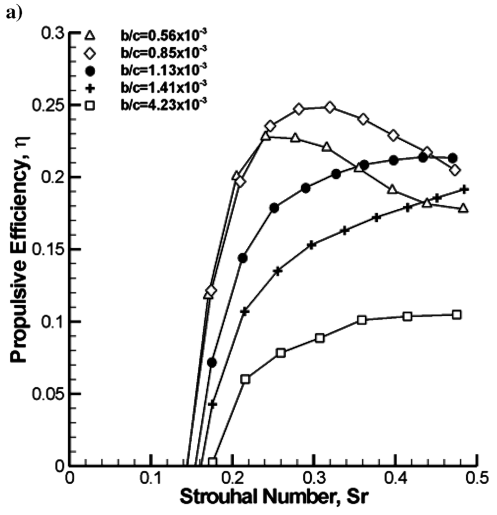

b)

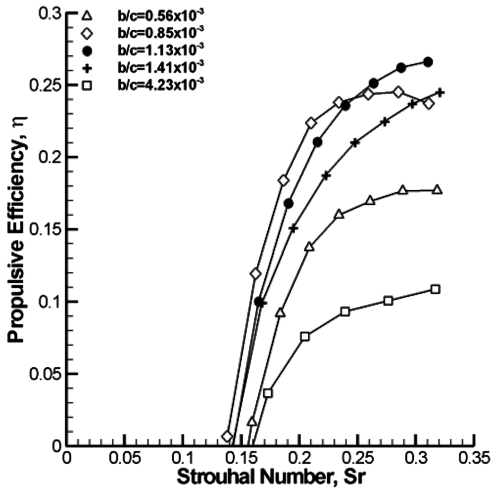

c)

Fig. 13 Propulsive efficiency as a function of Strouhal number: a) $Re = 9,000$; b) $Re = 18,000$; c) $Re = 27,000$.

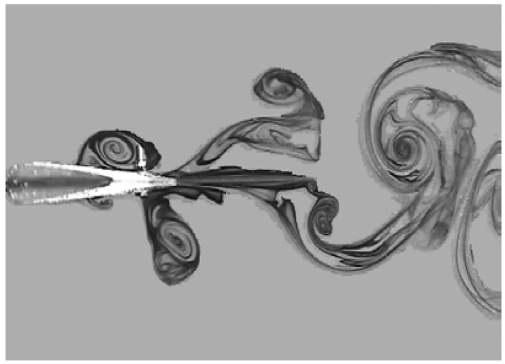

a)

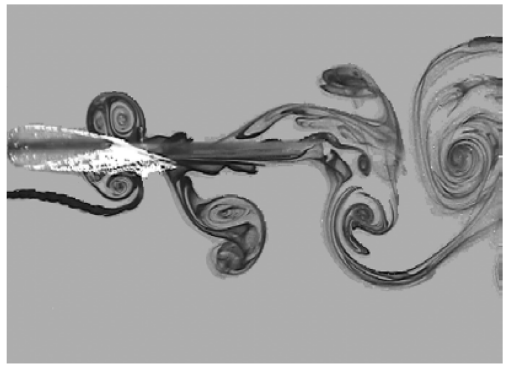

b)

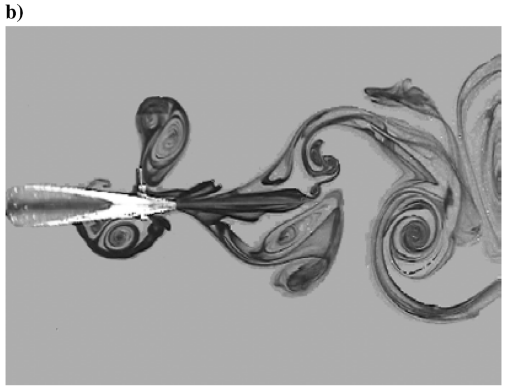

c)

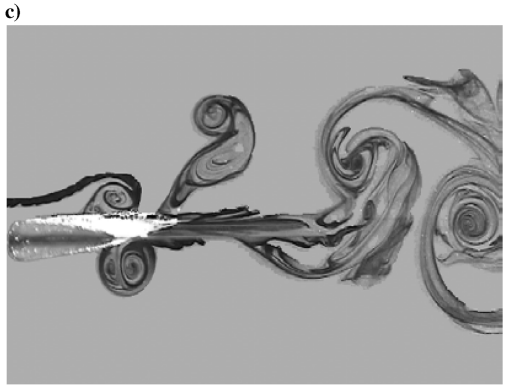

d)

Fig. 14 Dye flow visualization of vortices; $Re = 1,800$, $Sr = 0.29$, $b/c = 4.23 \times 10^{-3}$: a) $t/T = 0$; b) $t/T = \frac{1}{4}$; c) $t/T = \frac{1}{2}$; d) $t/T = \frac{3}{4}$.

0.34 is plotted in Fig. 16. The y coordinates (see Fig. 1) of the leading and trailing edges, and of the difference between them, $s_{\mathrm{LE}} - s_{\mathrm{TE}}$, are plotted as functions of time. It is seen that the trailing-edge trails the leading-edge in phase, whereas $s_{\mathrm{LE}} - s_{\mathrm{TE}}$ is seen to lead the leading edge. From Fig. 1, it is seen that the tangent of the pitch angle is equal to $s_{\mathrm{LE}} - s_{\mathrm{TE}}$ divided by the streamwise separation of the leading and trailing edges. The pitch phase angle is found by finding the phase of this new quantity relative to the leading edge. In the particular case illustrated in Fig. 16, the pitch phase angle is found to be 92.2 deg. The finding of a pitch phase angle of this value is of interest because phase angles of 90 deg have been found in the literature to optimize efficiency [15,17].

Pitch amplitude, pitch phase angle, and trailing-edge amplitude are plotted against the Strouhal number in Fig. 17. In addition to the specific case just discussed ($Re = 9,000$, $b/c = 0.56 \times 10^{-3}$), curves are also drawn for $b/c = 0.85 \times 10^{-3}$, $b/c = 1.13 \times 10^{-3}$,

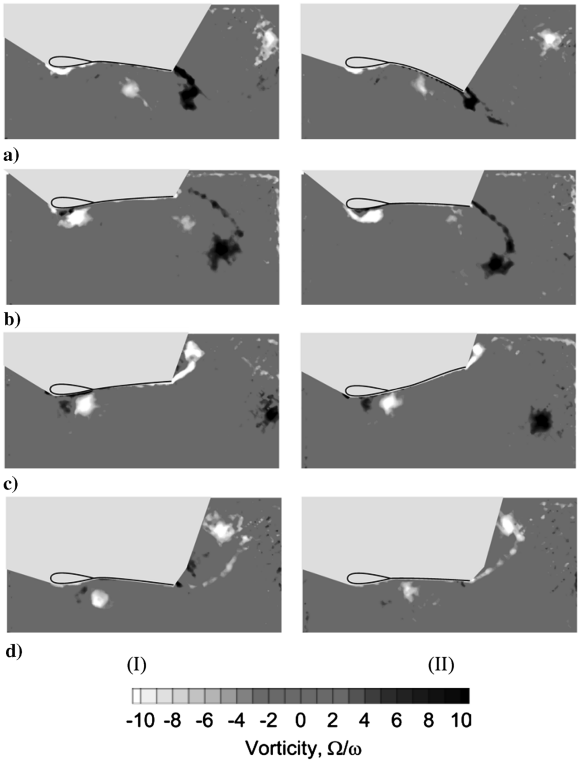

Fig. 15 Instantaneous vorticity; $Re = 9,000$, $Sr = 0.34$. I) $b/c = 0.85 \times 10^{-3}$, maximizes thrust; II) $b/c = 0.56 \times 10^{-3}$, maximizes efficiency: a) $t/T = 0$; b) $t/T = \frac{1}{4}$; c) $t/T = \frac{1}{2}$; d) $t/T = \frac{3}{4}$.

and $b/c = 1.41 \times 10^{-3}$. It is seen from Fig. 17a that, as a consequence of the inertia of the fluid, the pitch amplitude increases with increasing oscillation frequency and increasing flexibility. Pitch phase angle is plotted in Fig. 17b. It is seen that the pitch phase angle is always positive, indicating that the pitching motion of the airfoil always leads the heaving motion. The pitch phase angle is seen to increase with increasing plate thickness. The amplitude of the trailing edge is plotted against oscillation frequency in Fig. 17c. Trailing-edge amplitude is not an independent quantity, but is a function of pitch amplitude and pitch phase angle. With reference to Fig. 1, a pitch phase angle of zero degrees gives maximum positive ($s_{TE} < s_{LE}$) pitch angle when $s_{LE} = +a$. A pitch phase angle of 180 deg gives a maximum negative pitch angle when $s_{LE} = +a$. A 180 deg pitch phase angle is therefore favorable if a high trailing-edge amplitude is sought. At low Strouhal numbers the pitch phase angle is favorable. However, the pitch amplitude is very small, leading to a trailing-edge amplitude approximately equal to the leading-edge amplitude. At high Strouhal numbers the pitch amplitude is favorable and the pitch phase angle is unfavorable. Peaks in trailing-edge amplitude are observed at intermediate Strouhal numbers.

As stated above, the thrust coefficient may be plotted against a shape characteristic of the airfoil, rather than against plate thickness.

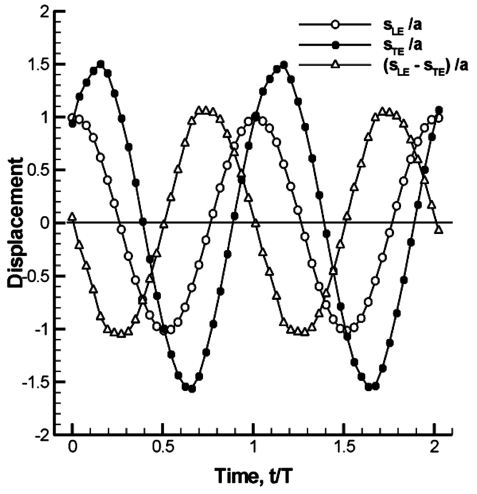

Fig. 16 Leading-edge displacement, trailing-edge displacement, and deformation as a function of time; $Re = 9,000$, $b/c = 0.56 \times 10^{-3}$, $Sr = 0.34$.

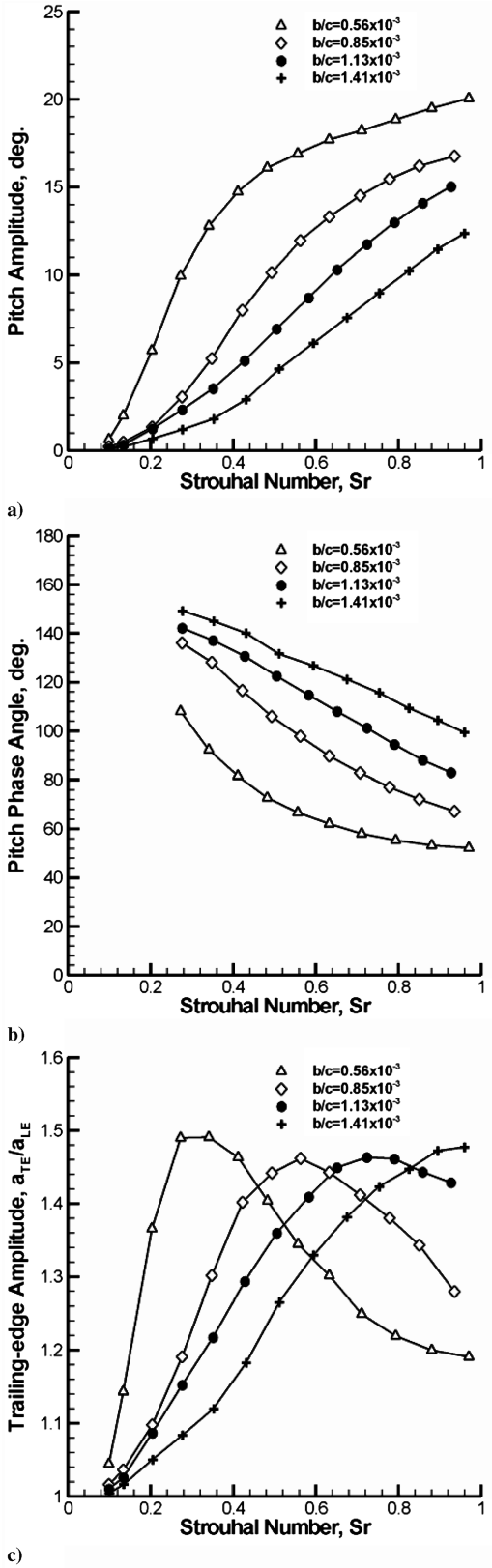

Fig. 17 The variation with Strouhal number of a) pitch amplitude; b) pitch phase angle; and c) trailing-edge amplitude, $Re = 9,000$.

It appears at first that three possibilities exist: pitch amplitude, pitch phase angle, and trailing-edge amplitude. When these quantities are plotted against each other an interesting pattern emerges. Pitch amplitude is plotted against pitch phase angle in Fig. 18a. Data for airfoils with $b/c = 0.56 \times 10^{-3}$, 0.85×10^{-3}, 1.13×10^{-3}, 1.41×10^{-3}, and 4.23×10^{-3} are plotted for $Re = 9,000$, 18,000, and 27,000, and for all Strouhal numbers. The direction of increasing flexibility and oscillation frequency is indicated. It is seen that pitch amplitude and pitch phase angle are dependent. Pitch amplitude varies almost linearly with pitch phase, with a gradient of -0.18 ± 0.02. It is noted that the experimental scatter is greatest in the small pitch-amplitude region. This is because of the difficulty in measuring the phase of small amplitude oscillations accurately. The trailing-edge amplitude is plotted against pitch phase angle in Fig. 18b. It is seen that the two quantities are dependent. For high pitch phase angles the pitch amplitude is very small (Fig. 18a), and the trailing-edge amplitude tends to the limit of unity. At low pitch phase angles the pitch amplitude is high but the phase is such that the airfoil pitches most steeply at an unfavorable point in the cycle; the trailing-edge amplitude is low again. At an intermediate pitch phase, of approximately 100 deg, the trailing-edge amplitude reaches a peak. In summary, it is seen that the three quantities, pitch amplitude, pitch phase angle, and trailing-edge amplitude, are dependent.

The question arises as to which parameter is most suitable to replace the plate thickness. Of the three possibilities, pitch phase angle, has been found throughout the literature to be of consistent significance. Furthermore, the value of the pitch phase angle that

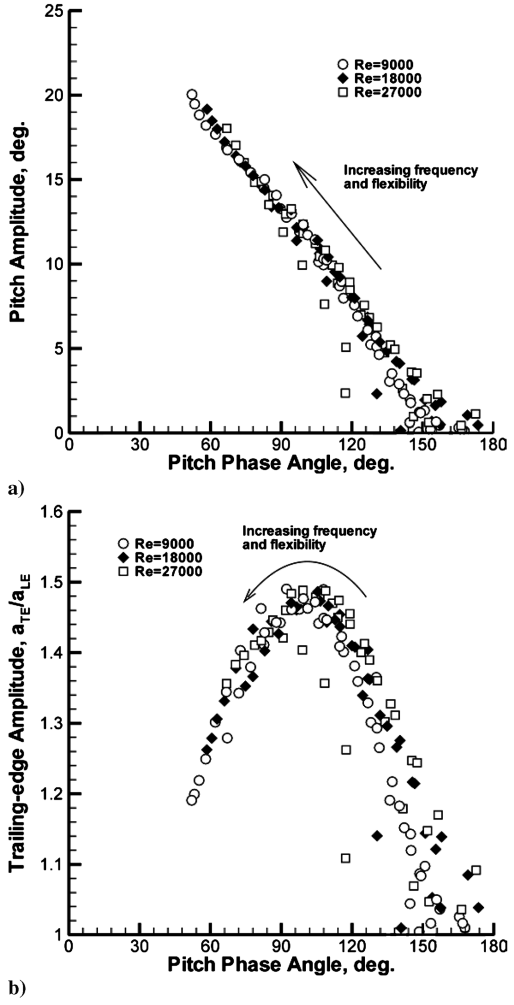

Fig. 18 a) Pitch amplitude as a function of pitch phase angle for the complete data set. The data points for all Reynolds numbers, airfoil thicknesses, and oscillation frequencies fall onto a line. b) Trailing-edge amplitude as a function of pitch phase angle. The data points fall onto a curve.

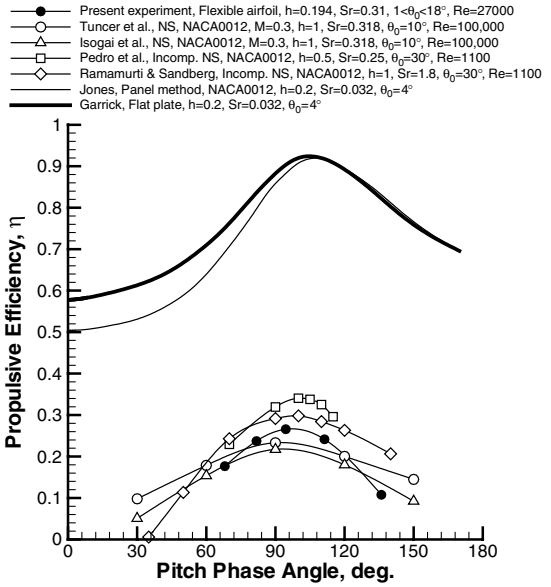

Fig. 19 Propulsive efficiency as a function of pitch phase angle. Comparison of present experimental results with linear theory, panel method, and both compressible and incompressible Navier–Stokes codes. The pitch amplitude θ_0 is variable for the present experiments, and fixed for all other data series. Optimum phase angles in the vicinity of 90 deg are found over a wide range of parameters.

maximizes efficiency has been found across a broad range of studies to lie in the region of 90 deg. For example, the rigid-airfoil Navier–Stokes analyses of Tuncer and Kaya [17], Isogai et al. [15], Tuncer et al. [52], Ramamurti and Sandberg [53], and Pedro et al. [29] predict optimum pitch phase angles of 86, 90, 90, 90–100, and 90–110 deg, respectively; in nature it is observed that pitch oscillations of the fin lead the heave motion by an angle close to 90 deg [54]; experimentally, Anderson [22] found high efficiencies for pitch phase angles of 75 and 90 deg, whereas Read et al. [55] found high efficiencies in the region of 90–100 deg. The common finding in the Navier–Stokes studies is that pitch phase angles in this range tend to lower the effective angle of attack amplitude, thus lessening the degree of leading-edge flow separation. Propulsive efficiency curves from a selection of these analyses, as well as the prediction of Garrick theory and a panel method from Jones [50], are plotted in Fig. 19. Note that, although the Reynolds number, Strouhal number, and amplitudes differ greatly, the optimum pitch phase angle is around 90 deg for each data set. Also shown in the figure is a curve from the present set of data, in which each data point corresponds to a different plate thickness. The similarity of the shape of the efficiency curve for the present data set to those of the studies of rigid airfoils in coupled heave and pitch, and the closeness of the optimum pitch phase angle to those in the other studies, suggests that the pitch phase angle is a suitable alternative parameter to the plate thickness. The performance of the airfoil may now be analyzed in terms of the Strouhal number and pitch phase angle.

E. Effect of Pitch Phase Angle and Strouhal Number

When thrust coefficient and propulsive efficiency are plotted against pitch phase angle an interesting pattern emerges: curves of constant Strouhal number tend to fall onto each other. Example plots are shown in Fig. 20. In part a), thrust coefficient curves for $Sr = 0.33$ and $Sr = 0.49$ are drawn; efficiency curves are shown in part b). It is seen that the effect of Reynolds number is small, as seen earlier for the NACA0012 airfoil.

The complete data set is represented as contour plots in Fig. 21 for thrust coefficient [part a)] and efficiency [part b)]. Contours of thrust coefficient are drawn on a pitch phase angle—Strouhal number plane in part a). The white curve indicates the optimum pitch phase angle (in terms of thrust) for a given Strouhal number. For a Strouhal number of $Sr = 0.29$, for example, the optimum pitch phase angle is 110 ± 4 deg. An airfoil of this flexibility would experience a higher

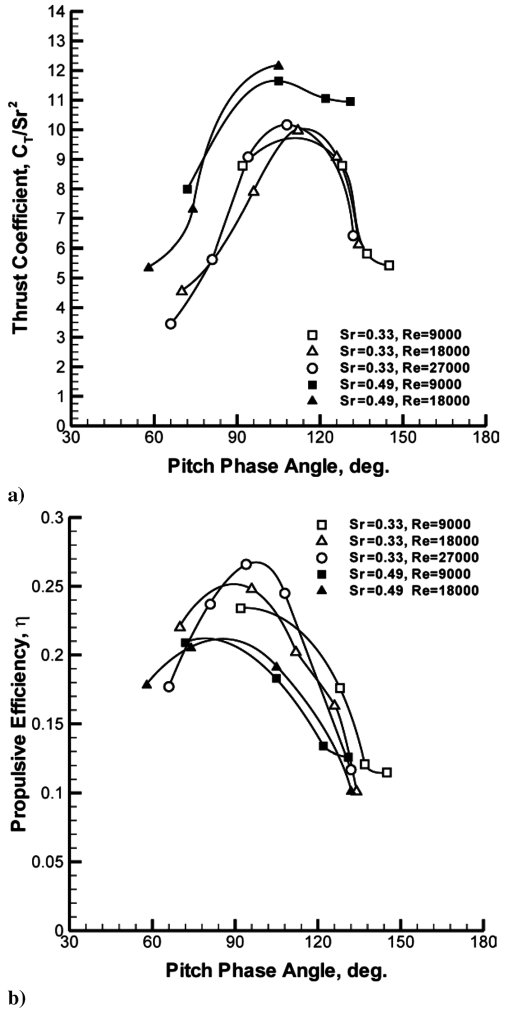

Fig. 20 The variation with pitch phase angle of a) thrust coefficient and b) propulsive efficiency. Curves are shown for $Sr = 0.33$ (open symbols) and $Sr = 0.49$ (solid symbols).

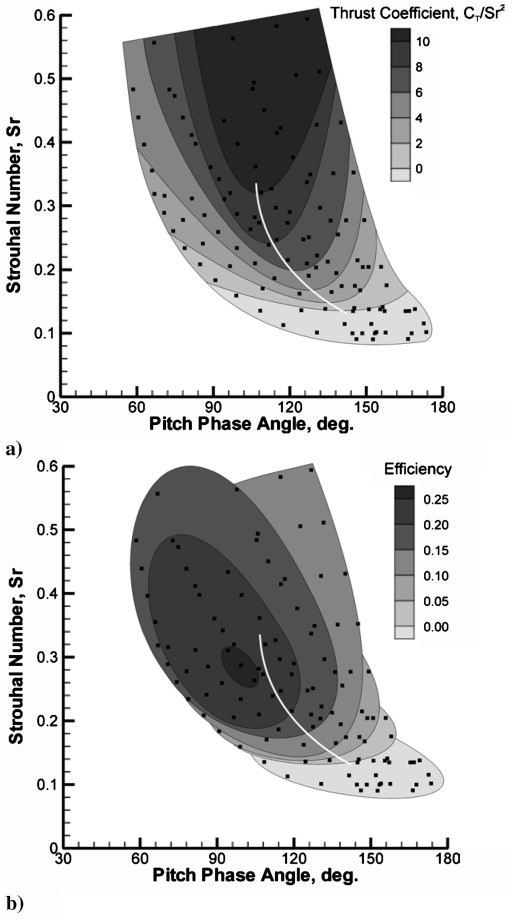

Fig. 21 Contours of a) thrust coefficient and b) propulsive efficiency, in the Strouhal number–pitch phase angle plane. Black dots indicate experimental data points. The complete set of data is plotted (all stiffnesses, frequencies, and Reynolds numbers). The solid white line indicates the peak thrust coefficient for a given Strouhal number.

thrust coefficient than a less flexible airfoil (the region to the right of the white curve), or a more flexible airfoil (the area to the left). The optimum pitch phase angle is observed to decrease as the Strouhal number increases. From a design aspect, the plot indicates the optimum pitch phase angle for a given flight Strouhal number. The optimum pitch phase angle may be compared with values from the literature. Tuncer and Kaya [17], Pedro et al. [29], Ramamurti and Sandberg [53], and Isogai et al. [15] observed optimum (in terms of thrust) pitch phase angles of 100, 115, 120, and 120 deg, respectively. It is seen from Fig. 21a that these values are in agreement with those found in the present experiment. The corresponding plot for propulsive efficiency is shown in Fig. 21b. The contour map exhibits a peak in efficiency at a Strouhal number of $Sr = 0.29$. It is noted that this lies within the range of Strouhal numbers of $0.2 < Sr < 0.4$ found in nature [44]. It may also be compared with the optimum Strouhal number $Sr = 0.30$ found experimentally by Anderson [22]. The reason for the decrease in efficiency for lower or higher Strouhal numbers may be attributed to the increase in flow separation at higher Strouhal numbers (higher effective angles of attack), and a transition to drag at lower Strouhal numbers. The optimum pitch phase angle is seen from Fig. 21b to be 100 ± 4 deg, consistent with the values found in studies of rigid airfoils in coupled heave and pitch, and those found in nature. It is noted that the angles found to optimize the thrust coefficient, both in the literature and in the present study, are higher than those found to maximize the efficiency. This is consistent with the observation [17] that it is not generally possible to achieve maximum thrust and efficiency simultaneously.

V. Conclusions

Water tunnel experiments on chordwise-flexible airfoils heaving with constant amplitude have been carried out for Reynolds numbers of 9,000 to 27,000. The results revealed peaks in thrust coefficient for intermediate stiffness at constant Strouhal number. These indicate that a degree of flexibility is beneficial from a thrust aspect. In the cases of higher thrust, the vortices are stronger and farther apart in the cross-stream direction. Also, the time-averaged flow fields showed a stronger jet. The effect of Strouhal number is similar to that of flexibility. Peaks in thrust coefficient are observed, which move to higher Strouhal numbers with increasing stiffness. Stronger vortices and time-averaged jets are observed for these optimum cases.

Efficiency benefits were also observed over a broad range of chordwise flexibility, with the optimum efficiency exceeding the efficiency of the inflexible airfoil by approximately 15%. Flow visualization and PIV data experiments revealed weaker leading-edge vortices in the cases of optimum efficiency.

An analogy was made between a flexible airfoil oscillating in heave and a rigid airfoil oscillating in pitch and heave. The three shape characteristics, pitch phase angle, pitch amplitude, and trailing-edge amplitude, were found to be interdependent. Data from measurements for all Reynolds numbers, plate thicknesses, and heave frequencies, were found to lie on a line (pitch amplitude vs pitch phase angle) or a curve (trailing-edge amplitude vs pitch phase angle). The phase angle of the pitch was found to lead the heaving motion.

Thrust coefficient and propulsive efficiency were found to be functions of Strouhal number and pitch phase angle. Contour plots of efficiency in the Strouhal number–pitch phase angle plane showed a

distinct peak for a pitch phase angle of 95–100 deg (consistent with experimental and Navier–Stokes analyses of rigid airfoils in coupled heave and pitch), and a Strouhal number of 0.29 (within the range $0.2 < Sr < 0.4$ observed in nature). Contours of thrust coefficient showed thrust to peak for pitch phase angles in the region of 110–120 deg, but at higher Strouhal numbers. The results suggest the effect of chordwise flexibility is beneficial for purely heaving airfoils at low Reynolds numbers.

Acknowledgment

This work has been supported by an Engineering and Physical Sciences Research Council studentship.

References

[1] Pornsin-sirirak, T. N., Tai, Y. C., Nassef, H., and Ho, C. M., "Titanium-Alloy MEMS Wing Technology for a Micro Aerial Vehicle Application," *Sensors and Actuators A (Physical)*, Vol. 89, No. 1–2, 2001, pp. 95–103.

[2] Peterson, B., Erath, B., Henry, K., Lyon, M., Walker, B., Powell, N., Fowkes, K., and Bowman, W. J., "Development of a Micro Air Vehicle for Maximum Endurance and Minimum Size," AIAA Paper 2003-416, 2003.

[3] Ifju, P. G., Jenkins, D. A., Ettinger, S., Lian, Y., Shyy, W., and Waszak, M. R., "Flexible-Wing-Based Micro Air Vehicles," AIAA Paper 2002-0705, 2002.

[4] Spedding, G. R., and Lissaman P. B. S., "Technical Aspects of Microscale Flight Systems," *Journal of Avian Biology*, Vol. 29, No. 4, 1998, pp. 458–468.

[5] Mueller, T. J., and DeLaurier, J. D., "Aerodynamics of Small Vehicles," *Annual Review of Fluid Mechanics*, Vol. 35, Jan. 2003, pp. 89–111.

[6] Knoller, R., "Die Gesetze des Luftwiderstandes (The Laws of Wind Resistance)," *Flug-und Motortechnik (Wien)*, Vol. 3, No. 21, 1909, pp. 1–7.

[7] Betz, A., "Ein Beitrag zur Erklaerung des Segelfluges (A Paper to Explain Glider Flight)," *Zeitschrift fuer Flugtechnik und Motorluftschiffahrt*, Vol. 3, No. 21, 1912, pp. 269–272.

[8] Katzmayr, R., "Effect of Periodic Changes of Angle of Attack on Behaviour of Airfoils," NACA 147, 1922.

[9] Garrick, I. E., "Propulsion of a flapping and oscillating airfoil," NACA 567, 1936.

[10] Wu, T. Y., "Hydromechanics of Swimming Propulsion, Part 2: Some Optimum Shape Problems," *Journal of Fluid Mechanics*, Vol. 46, No. 3, 1971, pp. 521–544.

[11] Lighthill, M. J., "Aquatic Animal Propulsion of High Hydromechanical Efficiency," *Journal of Fluid Mechanics*, Vol. 44, No. 2, 1970, pp. 265–301.

[12] Chopra, M. G., "Large Amplitude Lunate-Tail Theory of Fish Locomotion," *Journal of Fluid Mechanics*, Vol. 74, No. 1, 1976, pp. 161–182.

[13] Jones, K. D., Dohring, C. M., and Platzer, M. F., "Experimental and Computational Investigation of the Knoller–Betz Effect," *AIAA Journal*, Vol. 36, No. 7, 1998, pp. 1240–1246.

[14] Bhaskaran, R., and Rothmayer, A. P., "Separation and Instabilities in the Viscious Flow over Airfoil Leading Edges," *Computers and Fluids*, Vol. 27, No. 8, 1998, pp. 903–921.

[15] Isogai, K., Shinmoto, Y., and Watanabe, H., "Effects of Dynamic Stall on Propulsive Efficiency and Thrust of Flapping Airfoil," *AIAA Journal*, Vol. 37, No. 10, 1999, pp. 1145–1151.

[16] Tuncer, I. H., and Platzer, M. F., "Computational Study of Flapping Airfoil Aerodynamics," *Journal of Aircraft*, Vol. 37, No. 3, 2000, pp. 514–520.

[17] Tuncer, I. H., and Kaya, M., "Optimization of Flapping Airfoils for Maximum Thrust and Propulsive Efficiency," *AIAA Journal*, Vol. 43, No. 11, 2005, pp. 2329–2336.

[18] Lewin, G. C., and Haj-Hariri, H., "Modelling Thrust Generation of a Two-Dimensional Heaving Airfoil in a Viscous Flow," *Journal of Fluid Mechanics*, Vol. 492, Sept. 2003, pp. 339–362.

[19] Freymuth, P., "Thrust Generation by an Airfoil in Hover Modes," *Experiments in Fluids*, Vol. 9, Jan. 1990, pp. 17–24.

[20] Sunada, S., Kawachi, K., Matsumoto, A., and Sakaguchi, A., "Unsteady Forces on a Two-Dimensional Wing in Plunging and Pitching Motions," *AIAA Journal*, Vol. 39, No. 7, 2001, pp. 1230–1239.

[21] Lai, J. C. S., and Platzer, M. F., "Characteristics of a Plunging Airfoil at Zero Freestream Velocity," *AIAA Journal*, Vol. 39, No. 3, 2001, pp. 531–534.

[22] Anderson, J. M., Streitlien, K., Barrett, D. S., and Triantafyllou, M. S., "Oscillating Foils of High Propulsive Efficiency," *Journal of Fluid Mechanics*, Vol. 360, 1998, pp. 41–72.

[23] Bohl, D. G., and Koochesfahani, M. M., "MTV Measurements of the Flow Structure Downstream of an Oscillating Airfoil," AIAA Paper 2003-4017, 2003.

[24] Lai, J. C. S., and Platzer, M. F., "Jet Characteristics of a Plunging Airfoil," *AIAA Journal*, Vol. 37, No. 12, 1999, pp. 1529–1537.

[25] Heathcote, S., and Gursul, I., "Jet Switching Phenomenon for a Plunging Airfoil," AIAA Paper 2004-2150, 2004.

[26] Ihara, A., and Watanabe, H., "On the Flow Around Flexible Plates: Oscillating with Large Amplitude," *Journal of Fluids and Structures*, Vol. 8, No. 6, 1994, pp. 601–619.

[27] Koochesfahani, M. M., "Vortical Patterns in the Wake of an Oscillating Airfoil," *AIAA Journal*, Vol. 27, No. 9, 1989, pp. 1200–1205.

[28] Hover, F. S., Haugsdal, O., and Triantafyllou, M. S., "Effect of Angle of Attack Profiles in Flapping Foil Propulsion," *Journal of Fluids and Structures*, Vol. 19, No. 1, 2004, pp. 37–47.

[29] Pedro, G., Suleman, A., and Djilali, N., "A Numerical Study of the Propulsive Efficiency of a Flapping Hydrofoil," *International Journal for Numerical Methods in Fluids*, Vol. 42, No. 5, 2003, pp. 493–526.

[30] Sfakiotakis, M., Lane, D. M., and Davies, J. B. C., "Review of Fish Swimming Modes for Aquatic Locomotion," *IEEE Journal of Oceanic Engineering*, Vol. 24, No. 2, 1999, pp. 237–251.

[31] Wootton, R. J., "Support and Deformability in Insect Wings," *Journal of Zoology: Proceedings of the Zoological Society of London*, Vol. 193, 1981, pp. 447–468.

[32] Steppan, S. J., "Flexural Stiffness Patterns of Butterfly Wings (Papilionoidea)," *Journal of Research on the Lepidoptera*, Vol. 35, March 2000, pp. 61–77.

[33] Maxworthy, T., "The Fluid Dynamics of Insect Flight," *Annual Review of Fluid Mechanics*, Vol. 13, Jan. 1981, pp. 329–350.

[34] Triantafyllou, M. S., Triantafyllou, G. S., and Yue, D. K. P., "Hydrodynamics of Fishlike Swimming," *Annual Review of Fluid Mechanics*, Vol. 32, Jan. 2000, pp. 33–53.

[35] Katz, J., and Weihs, D., "Hydrodynamic Propulsion by Large Amplitude Oscillation of an Airfoil with Chordwise Flexibility," *Journal of Fluid Mechanics*, Vol. 88, No. 3, 1978, pp. 485–497.

[36] Murray, M. M., and Howle, L. E., "Spring Stiffness Influence on an Oscillating Propulsor," *Journal of Fluids and Structures*, Vol. 17, No. 7, 2003, pp. 915–926.

[37] Miao, J.-M., and Ho, M.-H., "Effect of Flexure on Aerodynamic Propulsive Efficiency of Flapping Flexible Airfoil," *Journal of Fluids and Structures* (to be published).

[38] Bozkurttas, M., Dong, H., Mittal, R., Madden, P., and Lauder, G. V., "Hydrodynamic Performance of Deformable Fish Fins and Flapping Foils," AIAA Paper 2006-1392, 2006.

[39] Heathcote, S., Martin, D., and Gursul, I., "Flexible Flapping Airfoil Propulsion at Zero Freestream Velocity," *AIAA Journal*, Vol. 42, No. 22, 2004, pp. 2196–2205.

[40] Jones, K. D., and Platzer, M. F., "Experimental Investigation of the Aerodynamic Characteristics of Flapping-Wing Micro Air Vehicles," AIAA Paper 2003-0418, 2003.

[41] Prempraneerach, P., Hover, F. S., and Triantafyllou, M. S., "The Effect of Chordwise Flexibility on the Thrust and Efficiency of a Flapping Foil," *Proceedings of the Thirteenth International Symposium on Unmanned Untethered Submersible Technology*, Autonomous Undersea Systems Institute, Lee, NH, 2003.

[42] Jones, K. D., Duggan, S. J., and Platzer, M. F., "Flapping-Wing Propulsion for a Micro Air Vehicle," AIAA Paper 2001-0126, 2001.

[43] Liu, H., Wassersug, R. J., and Kawachi, K., "A Computational Fluid Dynamics Study of Tadpole Swimming," *Journal of Experimental Biology*, Vol. 199, No. 6, 1996, pp. 1245–1260.

[44] Taylor, G. K., Nudds, R. L., and Thomas, A. L. R., "Flying and Swimming Animals Cruise at a Strouhal Number Tuned for High Power Efficiency," *Nature (London)*, Vol. 425, No. 6959, 2003, pp. 707–711.

[45] Murray, M. M., "Hydroelasticity Modeling of Flexible Propulsors," Ph. D. Dissertation, Mechanical Engineering and Materials Science Department, Duke Univ., Durham, NC, 2000.

[46] Frampton, K. D., Goldfarb, M., Monopoli, D., and Cveticanin, D., "Passive Aeroelastic Tailoring for Optimal Flapping Wings," *Fixed and Flapping Wing Aerodynamics for Micro Air Vehicle Applications*, edited by Mueller, T. J., Progress in Astronautics and Aeronautics, Vol. 185, AIAA, Reston, VA, 2001, pp. 473–482.

[47] Young, J., "Numerical Simulation of the Unsteady Aerodynamics of Flapping Airfoils," Ph.D. Dissertation, School of Aerospace, Civil and Mechanical Engineering, New South Wales Univ., Canberra, 2005.

[48] Young, J., and Lai, J. C. S., "Oscillation Frequency and Amplitude Effects on the Wake of a Plunging Airfoil," *AIAA Journal*, Vol. 42, No. 10, 2004, pp. 2042–2052.

[49] Sheldahl, R. E., and Klimas, P. C., "Aerodynamic Characteristics of Seven Symmetrical Airfoil Sections Through 180-Degree Angle of Attack for Use in Aerodynamic Analysis of Vertical Axis Wind Turbines," Sandia National Laboratories, Rept. SAND80-2114, 1981.

[50] Jones, K. D., Lund, T. C., and Platzer, M. F., "Experimental and Computational Investigation of Flapping Wing Propulsion for Micro Air Vehicles," *Fixed and Flapping Wing Aerodynamics for Micro Air Vehicle Applications*, edited by Mueller, T. J., Progress in Astronautics and Aeronautics, Vol. 195, AIAA, Reston, VA, 2001, pp. 307–339.

[51] Platzer, M. F., and Jones, K. D., "Flapping Wing Aerodynamics: Progress and Challenges," AIAA Paper 2006-500, 2006.

[52] Tuncer, I. H., Walz, R., and Platzer, M. F., "A Computational Study of the Dynamic Stall of a Flapping Airfoil," AIAA Paper 1998-2519, 1998.

[53] Ramamurti, R., and Sandberg, W. C., "Simulation of Flow About Flapping Airfoils Using Finite Element Incompressible Flow Solver," *AIAA Journal*, Vol. 39, No. 2, 2001, pp. 253–260.

[54] Rozhdestvensky, K. V., and Ryzhov, V. A., "Aerohydrodynamics of Flapping-Wing Propulsors," *Progress in Aerospace Sciences*, Vol. 39, No. 8, 2003, pp. 585–633.

[55] Read, D. A., Hover, F. S., and Triantafyllou, M. S., "Forces on Oscillating Foils for Propulsion and Maneuvering," *Journal of Fluids and Structures*, Vol. 17, No. 1, 2003, pp. 163–183.

F. Coton
Associate Editor